Available online at www.sciencedirect.com

SciVerse ScienceDirect

Nuclear Physics B 871 (2013) 1–20

NUCLEAR PHYSICS B

www.elsevier.com/locate/nuclphysb

Prompt charm production in pp collisions at $\sqrt{s} = 7$ TeV ☆

LHCb Collaboration

Received 13 February 2013; accepted 18 February 2013

Available online 24 February 2013

Abstract

Charm production at the LHC in pp collisions at $\sqrt{s} = 7$ TeV is studied with the LHCb detector. The decays $D^0 \to K^-\pi^+$, $D^+ \to K^-\pi^+\pi^+$, $D^{*+} \to D^0(K^-\pi^+)\pi^+$, $D_s^+ \to \phi(K^-K^+)\pi^+$, $\Lambda_c^+ \to pK^-\pi^+$, and their charge conjugates are analysed in a data set corresponding to an integrated luminosity of 15 nb^{-1}. Differential cross-sections $\mathrm{d}\sigma/\mathrm{d}p_\mathrm{T}$ are measured for prompt production of the five charmed hadron species in bins of transverse momentum and rapidity in the region $0 < p_\mathrm{T} < 8$ GeV/c and $2.0 < y < 4.5$. Theoretical predictions are compared to the measured differential cross-sections. The integrated cross-sections of the charm hadrons are computed in the above p_T-y range, and their ratios are reported. A combination of the five integrated cross-section measurements gives

$$\sigma(c\bar{c})_{p_\mathrm{T}<8\ \mathrm{GeV}/c,\ 2.0<y<4.5} = 1419 \pm 12\,(\mathrm{stat}) \pm 116\,(\mathrm{syst}) \pm 65\,(\mathrm{frag})\ \mu\mathrm{b},$$

where the uncertainties are statistical, systematic, and due to the fragmentation functions.

1. Introduction

Measurements of the production cross-sections of charmed hadrons test the predictions of quantum chromodynamic (QCD) fragmentation and hadronisation models. Perturbative calculations of charmed hadron production cross-sections at next-to-leading order using the Generalized Mass Variable Flavour Number Scheme (GMVFNS) [1–6] and at fixed order with next-to-leading-log resummation (FONLL) [7–10] reproduce the cross-sections measured in the central rapidity region ($|y| \leqslant 1$) in $p\overline{p}$ collisions at $\sqrt{s} = 1.97$ TeV at the Fermilab Tevatron collider [11] and the cross-sections measured in the central rapidity region ($|y| < 0.5$) in pp collisions at $\sqrt{s} = 2.96$ TeV [12] and at $\sqrt{s} = 7$ TeV [13,14] at the CERN Large Hadron Collider (LHC).

☆ © CERN for the benefit of the LHCb Collaboration.

0550-3213/
http://dx.doi.org/10.1016/j.nuclphysb.2013.02.010

The LHCb detector at the LHC provides unique access to the forward rapidity region at these energies with a detector that is tailored for flavour physics. This paper presents measurements with the LHCb detector of D^0, D^+, D_s^+, D^{*+}, and Λ_c^+ production in the forward rapidity region $2.0 < y < 4.5$ in pp collisions at a centre-of-mass energy of 7 TeV. Throughout this article, references to specific decay modes or specific charmed hadrons also imply the charge conjugate mode. The measurements are based on 15 nb^{-1} of pp collisions recorded with the LHCb detector in 2010 with approximately 1.1 visible interactions per triggered bunch crossing.

Charmed hadrons may be produced at the pp collision point either directly or as feed-down from the instantaneous decays of excited charm resonances. They may also be produced in decays of b-hadrons. In this paper, the first two sources (direct production and feed-down) are referred to as *prompt*. Charmed particles from b-hadron decays are called *secondary* charmed hadrons. The measurements described here are the production cross-sections of prompt charmed hadrons. Secondary charmed hadrons are treated as backgrounds. No attempt is made to distinguish between the two sources of prompt charmed hadrons.

2. Experimental conditions

The LHCb detector [15] is a single-arm forward spectrometer covering the pseudorapidity range $2 < \eta < 5$, designed for the study of particles containing b or c quarks. The detector includes a high precision tracking system consisting of a silicon-strip vertex detector surrounding the pp interaction region, a large-area silicon-strip detector located upstream of a dipole magnet with a bending power of about 4 Tm, and three stations of silicon-strip detectors and straw drift-tubes placed downstream. The combined tracking system has a momentum resolution ($\Delta p/p$) that varies from 0.4% at 5 GeV/c to 0.6% at 100 GeV/c and an impact parameter (IP) resolution of 20 μm for tracks with high transverse momentum. Charged hadrons are identified using two ring-imaging Cherenkov detectors. Photon, electron, and hadron candidates are identified by a calorimeter system consisting of scintillating-pad and pre-shower detectors, an electromagnetic calorimeter, and a hadronic calorimeter. Muons are identified by a system composed of alternating layers of iron and multiwire proportional chambers. The trigger consists of a hardware stage, based on information from the calorimeter and muon systems, followed by a software stage that applies a full event reconstruction.

During the considered data taking period, the rate of bunch crossings at the LHCb interaction point was sufficiently small that the software stage of the trigger could process all bunch crossings. Candidate events passed through the hardware stage of the trigger without filtering. The software stage of the trigger accepted bunch crossings for which at least one track was reconstructed in either the silicon-strip vertex detector or the downstream tracking stations. The sample is divided into two periods of data collection. In the first 1.9 ± 0.1 nb^{-1} all bunch crossings satisfying these criteria were retained. In the subsequent 13.1 ± 0.5 nb^{-1} the trigger retention rate was limited to a randomly selected $(24.0 \pm 0.2)\%$ of all bunch crossings.

For simulated events, pp collisions are generated using PYTHIA 6.4 [16] with a specific LHCb configuration [17] that employs the CTEQ6L1 parton densities [18]. Decays of hadronic particles are described by EVTGEN [19] in which final state radiation is generated using PHOTOS [20]. The interaction of the generated particles with the detector and its response are implemented using the GEANT4 toolkit [21] as described in Ref. [22].

3. Analysis strategy

The analysis is based on fully reconstructed decays of charmed hadrons in the following decay modes: $D^0 \to K^-\pi^+$, $D^+ \to K^-\pi^+\pi^+$, $D^{*+} \to D^0(K^-\pi^+)\pi^+$, $D_s^+ \to \phi(K^-K^+)\pi^+$, and $\Lambda_c^+ \to pK^-\pi^+$. Formally, the $D^0 \to K^-\pi^+$ sample contains the sum of the Cabibbo-favoured decays $D^0 \to K^-\pi^+$ and the doubly Cabibbo-suppressed decays $\overline{D}{}^0 \to K^-\pi^+$. For simplicity, we will refer to the combined sample by its dominant component.

The measurements are performed in two-dimensional bins of the transverse momentum ($p_{\rm T}$) and rapidity (y) of the reconstructed hadrons, measured with respect to the beam axis in the pp centre-of-mass (CM) frame. For the D^0, D^+, D^{*+}, and D_s^+ measurements, we use eight bins of uniform width in the range $0 < p_{\rm T} < 8$ GeV/c and five bins of uniform width in the range $2.0 < y < 4.5$. For the Λ_c^+ measurement, we partition the data in two ways: six uniform $p_{\rm T}$ bins in $2 < p_{\rm T} < 8$ GeV/c with a single $2.0 < y < 4.5$ bin and a single $2 < p_{\rm T} < 8$ GeV/c bin with five uniform y bins in $2.0 < y < 4.5$.

3.1. Selection criteria

The selection criteria were tuned independently for each decay. The same selection criteria are used for $D^0 \to K^-\pi^+$ candidates in the D^0 and D^{*+} cross-section measurements. We use only events that have at least one reconstructed primary interaction vertex (PV). Each final state kaon, pion, or proton candidate used in the reconstruction of a D^0, D^+, D_s^+, or Λ_c^+ candidate must be positively identified. Because of the relatively long lifetimes of the D^0, D^+, D_s^+, and Λ_c^+ hadrons, the trajectories of their decay products will not, in general, point directly back to the PV at which the charmed hadron was produced. To exploit this feature, the selections for these decays require that each final state candidate has a minimum impact parameter χ^2 (IP χ^2) with respect to the PV. The IP χ^2 is defined as the difference between the χ^2 of the PV reconstructed with and without the considered particle. For the D^0 and Λ_c^+ reconstruction, a common IP χ^2 requirement is imposed on all final state particles. For the D^+ and D_s^+ candidates, progressively stricter limits are used for the three daughters. Final-state decay products of charmed hadrons have transverse momenta that are generally larger than those of stable charged particles produced at the PV. Applying lower limits on the $p_{\rm T}$ of the final state tracks suppresses combinatorial backgrounds in the selections of D^0, D^+, and Λ_c^+ samples.

The selections of candidate charmed hadron decays are further refined by studying properties of the combinations of the selected final state particles. Candidate $D_s^+ \to \phi(K^-K^+)\pi^+$ decays are required to have a K^-K^+ invariant mass within ± 20 MeV/c^2 of the $\phi(1020)$ mass [23]. The decay products for each candidate charmed hadron must be consistent with originating from a common vertex with a good quality fit. The significant lifetimes of D^0, D^+, D_s^+, and Λ_c^+ hadrons are exploited by requiring that the fitted decay vertexes are significantly displaced from the PV. The trajectory of a prompt charmed hadron should point back to the PV in which it was produced. For D^0 candidates this is exploited as a requirement that IP $\chi^2 < 100$. For D^0 decays, we use one additional discriminating variable: the angle between the momentum of the D^0 candidate in the laboratory frame and the momentum of the pion candidate from its decay evaluated in the D^0 rest frame. The cosine of this angle has a flat distribution for D^0 decays but peaks strongly in the forward direction for combinatorial backgrounds. Candidate D^{*+} decays are reconstructed from D^0 and *slow* pion candidates. Figs. 1–3 show the invariant mass distributions and the $\log_{10}$(IP χ^2) distributions of the selected charmed hadron candidates.

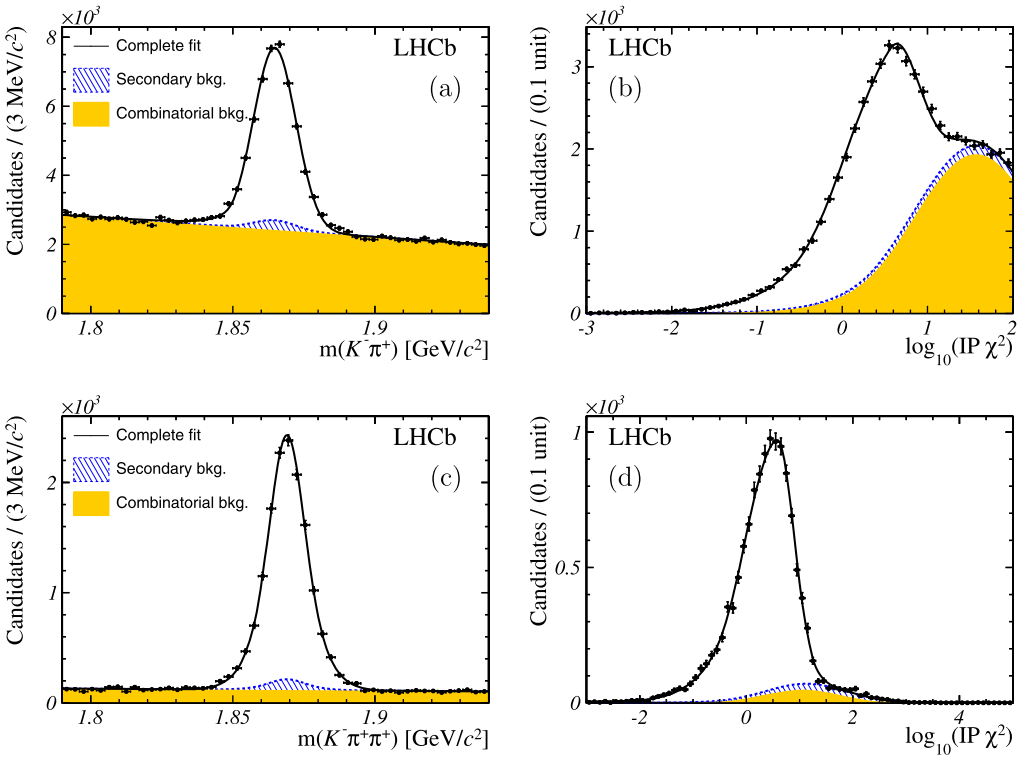

Fig. 1. Mass and $\log_{10}(\mathrm{IP}\,\chi^2)$ distributions for selected $D^0 \to K^-\pi^+$ and $D^+ \to K^-\pi^+\pi^+$ candidates showing (a) the masses of the D^0 candidates, (b) the $\log_{10}(\mathrm{IP}\,\chi^2)$ distribution of D^0 candidates for a mass window of ± 16 MeV/c^2 (approximately $\pm 2\sigma$) around the fitted $m(K^-\pi^+)$ peak, (c) the masses of the D^+ candidates, and (d) the $\log_{10}(\mathrm{IP}\,\chi^2)$ distribution of D^+ candidates for a mass window of ± 11 MeV/c^2 (approximately $\pm 2\sigma$) around the fitted $m(K^-\pi^+\pi^+)$ peak. Projections of likelihood fits to the full data samples are shown with components as indicated in the legends.

We factorise the efficiencies for reconstructing and selecting signal decays into components that are measured with independent studies. The particle identification (PID) efficiencies for pions, kaons, and protons are measured in data in bins of track p_{T} and pseudorapidity, η, using high purity samples of pions, kaons, and protons from K^0_s, $\phi(1020)$, and Λ decays. The effective total PID efficiency for each (p_{T}, y) bin of each charmed hadron decay mode is determined by calculating the average efficiency over the bin using these final state PID efficiencies and the final state (p_{T}, η) distributions from simulated decays. The efficiencies of the remaining selection criteria are determined from studies with the full event simulation.

3.2. *Determination of signal yields*

We use multidimensional extended maximum likelihood fits to the mass and $\log_{10}(\mathrm{IP}\,\chi^2)$ distributions to determine the prompt signal yields. For the $D^{*+} \to D^0\pi^+$ mode the $\log_{10}(\mathrm{IP}\,\chi^2)$ of the daughter D^0 is used. The selected candidates contain *secondary backgrounds* from signal decays produced in decays of b-hadrons and *combinatorial backgrounds*. The $D^{*+} \to D^0\pi^+$ decay has two additional sources of background from D^0 decays combined with unrelated slow pion candidates: *prompt random slow pion backgrounds* in which the D^0 mesons are produced at the

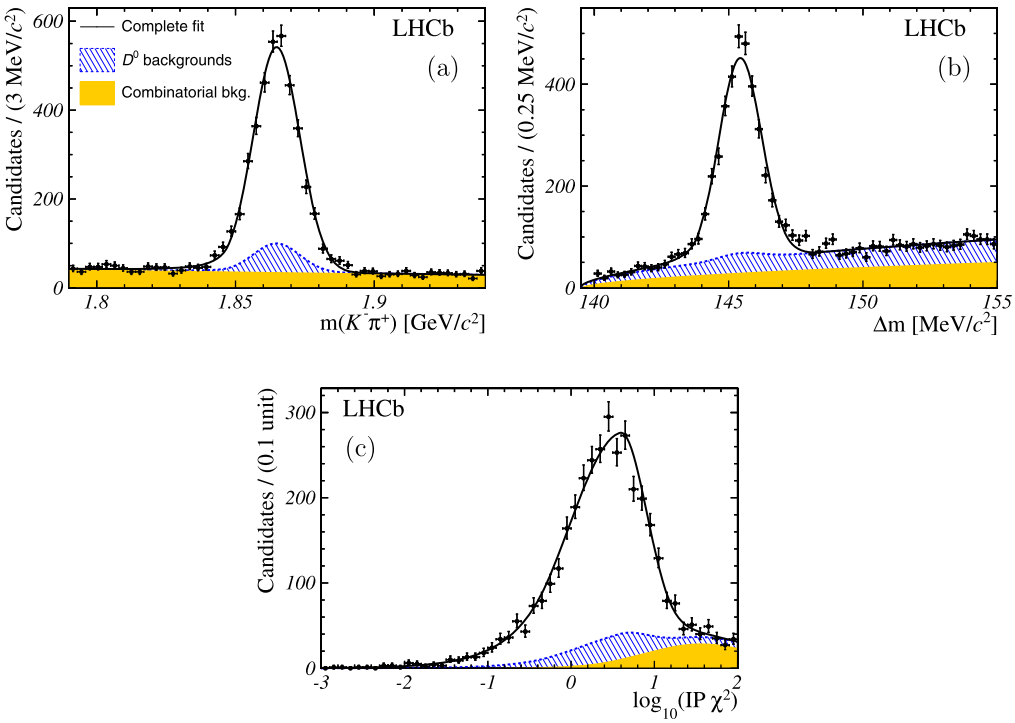

Fig. 2. Mass and $\log_{10}(\mathrm{IP}\,\chi^2)$ distributions for selected $D^{*+} \to D^0(K^-\pi^+)\pi^+$ candidates showing (a) the masses of the D^0 candidates for a window of ± 1.6 MeV/c^2 (approximately $\pm 2\sigma$) around the fitted Δm peak, (b) the differences between the D^{*+} and D^0 candidate masses for a mass window of ± 16 MeV/c^2 (approximately $\pm 2\sigma$) around the fitted $m(K^-\pi^+)$ peak, and (c) the $\log_{10}(\mathrm{IP}\,\chi^2)$ distribution of the D^0 candidate for a mass signal box of ± 16 MeV/c^2 around the fitted $m(K^-\pi^+)$ peak and ± 1.6 MeV/c^2 around the fitted Δm peak. Projections of a likelihood fit to the full data sample are shown with components as indicated in the legend. The 'D^0 backgrounds' component is the sum of the secondary, prompt random slow pion, and secondary random slow pion backgrounds.

PV and *secondary random slow pion backgrounds* in which the D^0 mesons are produced in decays of b-hadrons. The combinatorial backgrounds are separated from the remaining components with the reconstructed D^0, D^+, D_s^+, and Λ_c^+ mass distributions. Analysis of the $\log_{10}(\mathrm{IP}\,\chi^2)$ distributions allow separation of the prompt signal and secondary backgrounds. The additional random slow pion backgrounds in the $D^{*+} \to D^0(K^-\pi^+)\pi^+$ mode are identified in the distribution of the difference Δm between the masses of the D^{*+} and D^0 candidates. Thus the prompt signal yields for D^0, D^+, D_s^+, and Λ_c^+ decays are measured with two-dimensional fits to the mass and $\log_{10}(\mathrm{IP}\,\chi^2)$, and the prompt signal yields for D^{*+} decays are determined with three-dimensional fits to the D^0 candidate mass, Δm, and $\log_{10}(\mathrm{IP}\,\chi^2)$.

The extended likelihood functions are constructed from multidimensional probability density functions (PDFs). For each class of events, the multidimensional PDF is the product of an appropriate one-dimensional PDF in each variable:

Prompt signal: The mass distributions are represented by Crystal Ball functions [24] for D^0 decays (both direct and from D^{*+} mesons), double Gaussian functions for the D^+ and D_s^+ modes, and a single Gaussian function for the Λ_c^+ mode. The Δm distribution for

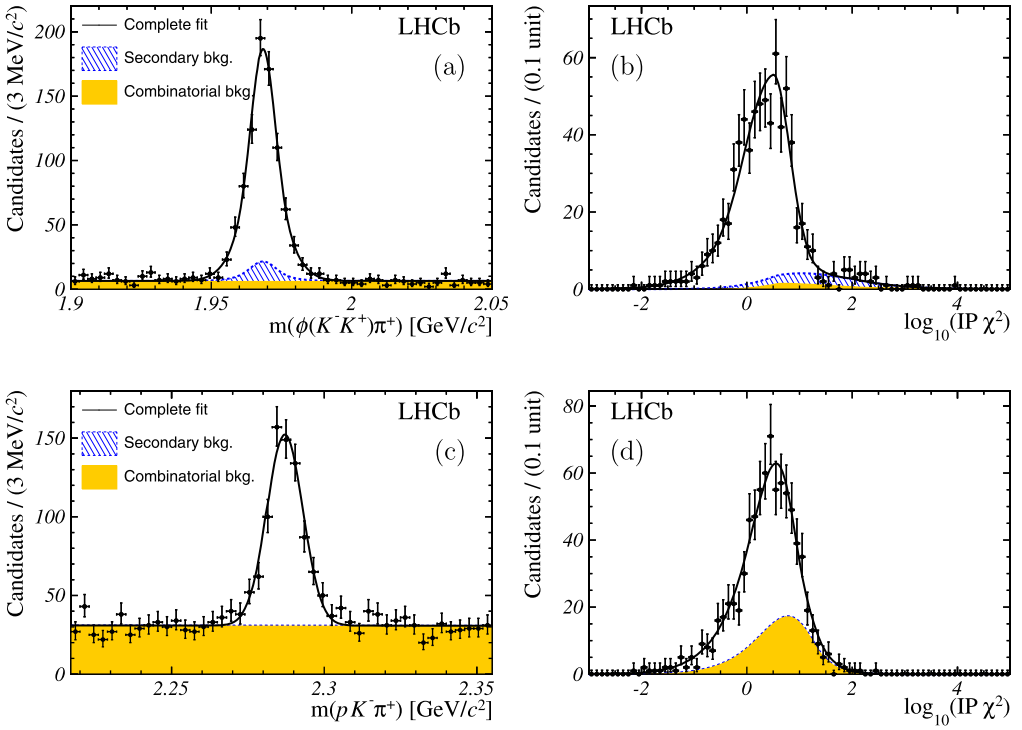

Fig. 3. Mass and $\log_{10}(\mathrm{IP}\,\chi^2)$ distributions for selected $D_s^+ \to \phi(K^-K^+)\pi^+$ and $\Lambda_c^+ \to pK^-\pi^+$ candidates showing (a) the masses of the D_s^+ candidates, (b) the $\log_{10}(\mathrm{IP}\,\chi^2)$ distribution of D_s^+ candidates for a mass window of ± 8 MeV/c^2 (approximately $\pm 2\sigma$) around the fitted $m(\phi(K^-K^+)\pi^+)$ peak, (c) the masses of the Λ_c^+ candidates, and (d) the $\log_{10}(\mathrm{IP}\,\chi^2)$ distribution of Λ_c^+ candidates for a mass window of ± 12 MeV/c^2 (approximately $\pm 2\sigma$) around the fitted $m(pK^-\pi^+)$ peak. Projections of likelihood fits to the full data samples are shown with components as indicated in the legends.

the D^{*+} mode is represented by a Crystal Ball function. The $\log_{10}(\mathrm{IP}\,\chi^2)$ distributions are represented by bifurcated Gaussian functions with exponential tails defined as

$$f_{\mathrm{BG}}(x;\mu,\sigma,\varepsilon,\rho_L,\rho_R) = \begin{cases} \exp\left(\frac{\rho_L^2}{2} + \frac{x-\mu}{\sigma\cdot(1-\varepsilon)}\cdot\rho_L\right) & \text{if } x < \mu - \rho_L\cdot\sigma\cdot(1-\varepsilon), \\ \exp\left(-\frac{(x-\mu)^2}{2\cdot\sigma^2\cdot(1-\varepsilon)^2}\right) & \text{if } \mu - \rho_L\cdot\sigma\cdot(1-\varepsilon) < x < \mu, \\ \exp\left(-\frac{(x-\mu)^2}{2\cdot\sigma^2\cdot(1+\varepsilon)^2}\right) & \text{if } \mu < x < \mu + \rho_R\cdot\sigma\cdot(1+\varepsilon), \\ \exp\left(\frac{\rho_R^2}{2} - \frac{x-\mu}{\sigma\cdot(1+\varepsilon)}\cdot\rho_R\right) & \text{if } \mu + \rho_R\cdot\sigma\cdot(1+\varepsilon) < x, \end{cases} \quad (1)$$

where μ is the mode of the distribution, σ is the average of the left and right Gaussian widths, ε is the asymmetry of the left and right Gaussian widths, and $\rho_{L(R)}$ is the exponential coefficient for the left (right) tail.

Secondary backgrounds: The functions representing the mass (and Δm) distributions are identical to those used for the prompt signal in each case. The $\log_{10}(\mathrm{IP}\,\chi^2)$ distributions are represented by f_{BG} functions.

Combinatorial backgrounds: The mass distributions are represented by first order polynomials. The $\log_{10}(\mathrm{IP}\,\chi^2)$ distributions are represented by f_{BG} functions. The Δm distribution for the D^{*+} mode is represented by a power-law function $C(\Delta m - M_\pi)^p$ where the exponent p is a free parameter; M_π is the pion mass and C is a normalisation constant.

Prompt random slow pion backgrounds (D^{*+} only): The functions representing the mass and $\log_{10}(\mathrm{IP}\,\chi^2)$ distributions are identical to those used for the prompt signal. The function representing the Δm distribution is the same power law function as that used for the combinatorial backgrounds.

Secondary random slow pion backgrounds (D^{*+} only): The functions representing the mass and $\log_{10}(\mathrm{IP}\,\chi^2)$ distributions are identical to those used for the secondary backgrounds. The function representing the Δm distribution is the same power law function as that used for the combinatorial backgrounds.

Shape parameters for the $\log_{10}(\mathrm{IP}\,\chi^2)$ distributions of combinatorial backgrounds are fixed based on fits to the mass sidebands. Those of the prompt signal, secondary backgrounds, and random slow pion backgrounds are fixed based on fits to simulated events. Figs. 1–3 show the results of single fits to the full $0 < p_{\mathrm{T}} < 8$ GeV/c, $2.0 < y < 4.5$ kinematic region.

The extended maximum likelihood fits are performed for each p_{T}-y bin. We simultaneously fit groups of adjacent bins constraining to the same value several parameters that are expected to vary slowly across the kinematic region. The secondary background component in the Λ_c^+ mode is too small to be measured reliably. We set its yield to zero when performing the fits and adopt a systematic uncertainty of 3% to account for the small potential contamination from secondary production.

3.3. Systematic uncertainties

There are three classes of systematic uncertainties: globally correlated sources, sources that are correlated between bins but uncorrelated between decay modes, and sources that are uncorrelated between bins and decay modes. The globally correlated contributions are the uncertainty on the measured luminosity and the uncertainty on the tracking efficiency. The former is a uniform 3.5% for each mode. The latter is 3% per final state track in the D^0, D^+, D_s^+, and Λ_c^+ measurements and 4% for the slow pion in the D^{*+} measurement. We adopt the uncertainty of the branching fractions as a bin-correlated systematic uncertainty. Systematic uncertainties of the reconstruction and selection efficiencies include contributions from the limited size of the simulated samples, failures in the association between generated and reconstructed particles in the simulation, differences between the observed and simulated distributions of selection variables, and differences between the simulated and actual resonance models in the D^+ and Λ_c^+ measurements. The yield determination includes uncertainties from the fit models, from peaking backgrounds due to mis-reconstructed charm cross-feed, and from potential variations in the yields of secondary backgrounds. Where possible, the sizes of the systematic uncertainties are evaluated independently for each bin. The sources of systematic uncertainties are uncorrelated, and the total systematic uncertainty in each bin of each mode is determined by adding the systematic uncertainties in quadrature. Table 1 summarises the systematic uncertainties.

As cross-checks, additional cross-section measurements are performed with the decay modes $D^0 \to K^-\pi^+\pi^-\pi^+$ and $D^+ \to \phi(K^-K^+)\pi^+$ and with a selection of $D^0 \to K^-\pi^+$ decays that does not use particle identification information. Their results are in agreement with the results from our nominal measurements.

Table 1
Overview of systematic uncertainties and their values, expressed as relative fractions of the cross-section measurements in percent (%). Uncertainties that are computed bin-by-bin are expressed as ranges giving the minimum to maximum values of the bin uncertainties. The correlated and uncorrelated uncertainties are shown as discussed in the text.

Source	D^0	D^{*+}	D^+	D_s^+	Λ_c^+
Selection and reconstruction (correlated)	1.6	2.6	4.3	5.3	0.4
(uncorrelated)	1–12	3–9	1–10	4–9	5–17
Yield determination (correlated)	2.5	2.5	0.5	1.0	3.0
(uncorrelated)	–	–	1–5	2–14	4–9
PID efficiency	1–5	1–5	6–19	1–15	5–9
Tracking efficiency	6	10	9	9	9
Branching fraction	1.3	1.5	2.1	5.8	26.0
Luminosity	3.5	3.5	3.5	3.5	3.5

4. Cross-section measurements

The signal yields determined from the data allow us to measure the differential cross-sections as functions of p_{T} and y in the range $0 < p_{\mathrm{T}} < 8$ GeV/c and $2.0 < y < 4.5$. The differential cross-section for producing hadron species H_c or its charge conjugate in bin i, $\mathrm{d}\sigma_i(H_c)/\mathrm{d}p_{\mathrm{T}}$, integrated over the y range of the bin is calculated with the relation

$$\frac{\mathrm{d}\sigma_i(H_c)}{\mathrm{d}p_{\mathrm{T}}} = \frac{1}{\Delta p_{\mathrm{T}}} \cdot \frac{N_i(H_c \to f + \mathrm{c.c.})}{\varepsilon_{i,\mathrm{tot}}(H_c \to f) \cdot \mathcal{B}(H_c \to f) \cdot \mathcal{L}_{\mathrm{int}}}, \tag{2}$$

where Δp_{T} is the width in p_{T} of bin i, typically 1 GeV/c, $N_i(H_c \to f + \mathrm{c.c.})$ is the measured yield of H_c and their charge conjugate decays in bin i, $\mathcal{B}(H_c \to f)$ is the branching fraction of the decay, $\varepsilon_{i,\mathrm{tot}}(H_c \to f)$ is the total efficiency for observing the signal decay in bin i, and $\mathcal{L}_{\mathrm{int}} = 15.0 \pm 0.5\ \mathrm{nb}^{-1}$ is the integrated luminosity of the sample. The following branching fractions from Ref. [23] are used: $\mathcal{B}(D^+ \to K^-\pi^+\pi^+) = (9.13 \pm 0.19)\%$, $\mathcal{B}(D^{*+} \to D^0(K^-\pi^+)\pi^+) = (2.63 \pm 0.04)\%$, $\mathcal{B}(\Lambda_c^+ \to pK^-\pi^+) = (5.0 \pm 1.3)\%$, and $\mathcal{B}((D^0 + \overline{D}^0) \to K^-\pi^+) = (3.89 \pm 0.05)\%$, where the last is the sum of Cabibbo-favoured and doubly Cabibbo-suppressed branching fractions. For the D_s^+ measurement we use the branching fraction of $D_s^+ \to K^-K^+\pi^+$ in a ± 20 MeV/c window around the $\phi(1020)$ mass: $\mathcal{B}(D_s^+ \to \phi(K^-K^+)\pi^+) = (2.24 \pm 0.13)\%$ [25]. The measured differential cross-sections are tabulated in Appendix A. Bins with a sample size insufficient to produce a measurement with a total relative uncertainty of less than 50% are discarded.

Theoretical expectations for the production cross-sectionsof charmed hadrons have been calculated by Kniehl et al. using the GMVFNS scheme [1–6] and Cacciari et al., using the FONLL approach [7–10]. Both groups have provided differential cross-sections as functions of p_{T} and integrated over bins in y.

The FONLL calculations use the CTEQ 6.6 [26] parameterisation of the parton densities. They include estimates of theoretical uncertainties due to the charm quark mass and the renormalisation and factorisation scales. However, we display only the central values in Figs. 4–5. The theoretical calculations assume unit transition probabilities from a primary charm quark to the exclusive hadron state. The actual transition probabilities that we use to convert the predictions to measurable cross-sections are those quoted by Ref. [27], based on measurements from e^+e^- colliders close to the $\Upsilon(4S)$ resonance: $f(c \to D^0) = 0.565 \pm 0.032$, $f(c \to D^+) = 0.246 \pm 0.020$, $f(c \to D^{*+}) = 0.224 \pm 0.028$, $f(c \to D_s^+) = 0.080 \pm 0.017$, and $f(c \to \Lambda_c^+) = 0.094 \pm 0.035$. Note that the transition probabilities do not sum up to unity, since, *e.g.*, $f(c \to D^0)$ has an

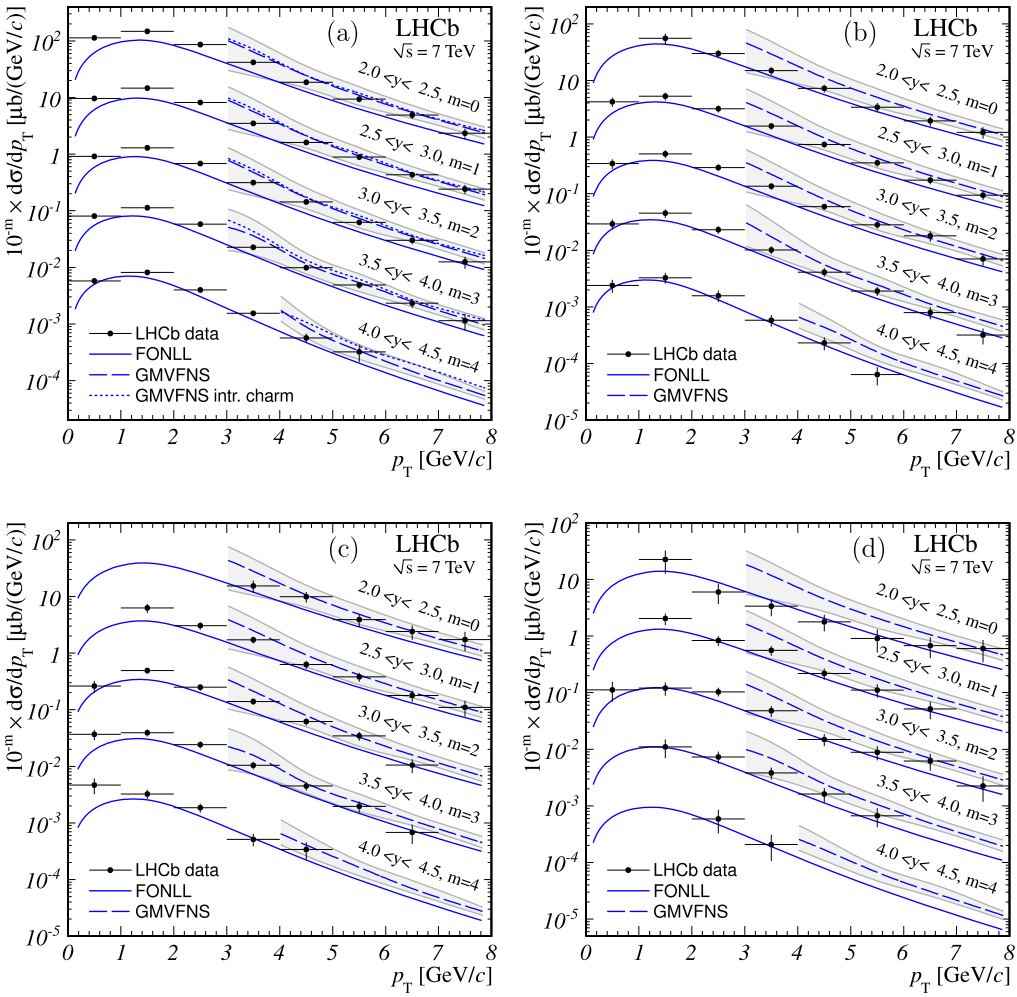

Fig. 4. Differential cross-sections for (a) D^0, (b) D^+, (c) D^{*+}, and (d) D_s^+ meson production compared to theoretical predictions. The cross-sections for different y regions are shown as functions of p_T. The y ranges are shown as separate curves and associated sets of points scaled by factors 10^{-m}, where the exponent m is shown on the plot with the y range. The error bars associated with the data points show the sum in quadrature of the statistical and total systematic uncertainty. The shaded regions show the range of theoretical uncertainties for the GMVFNS prediction.

overlapping contribution from $f(c \to D^{*+})$. No dedicated calculation for D_s^+ production is available. The respective prediction was obtained by scaling the kinematically similar D^{*+} prediction by the ratio $f(c \to D_s^+)/f(c \to D^{*+})$.

The GMVFNS calculations include theoretical predictions for all hadrons studied in our analysis. Results were provided for $p_T > 3$ GeV/c. The uncertainties from scale variations were determined only for the case of D^0 production. The relative sizes of the uncertainties for the other hadron species are assumed to be the same as those for the D^0. Here the CTEQ 6.5 [28] set of parton densities was used. Predictions for D^0 mesons were also provided using the CTEQ 6.5c2 [29] parton densities with intrinsic charm. As shown in Fig. 4(a), in the phase space region of the

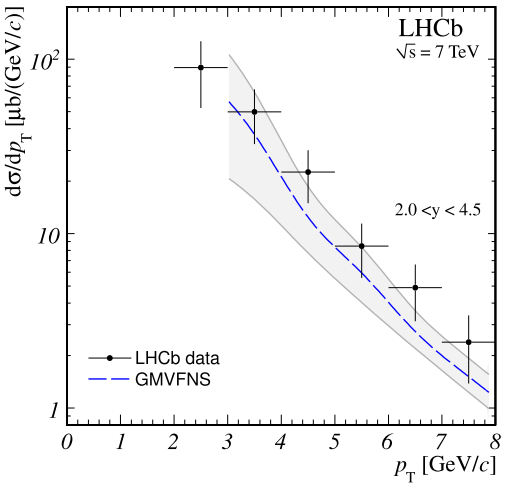

Fig. 5. Differential cross-sectionsfor Λ_c^+ baryon production compared to the theoretical prediction from the GMVFNS scheme. The error bars associated with the data points show the sum in quadrature of the statistical and total systematic uncertainty. The shaded region shows the range of theoretical uncertainty for the theoretical prediction.

present measurement the effect of intrinsic charm is predicted to be small. The GMVFNS theoretical framework includes the convolution with fragmentation functions describing the transition $c \to H_c$ that are normalised to the respective total transition probabilities [4]. The fragmentation functions are results of a fit to production measurements at e^+e^- colliders, where no attempt was made in the fit to separate direct production and feed-down from higher resonances.

To compare the theoretical calculations to our measurements, the theoretical differential cross-sections were integrated over the p_T bins and then divided by the bin width Δp_T. The integration was performed numerically with a third-order spline interpolation of the differential cross-sections.

The measured cross-sections compared to the theoretical predictions are shown in Figs. 4–5. For better visibility, theoretical predictions are displayed as smooth curves such that the value at the bin centre corresponds to the differential cross-section calculated in that bin. The data points with their uncertainties, which are always drawn at the bin centre, thus can be directly compared with theory. The predictions agree well with our measurements, generally bracketing the observed values between the FONLL and GMVFNS calculations.

5. Production ratios and integrated cross-sections

Charmed hadron production ratios and total cross-sections are determined for the kinematic range $0 < p_T < 8$ GeV/c and $2.0 < y < 4.5$. Bins where the relative uncertainty on the yield exceeds 50% (left blank in Tables 5–10 of Appendix A) are not used. Instead, the cross-sections are extrapolated from the remaining bins with predictions obtained from PYTHIA 6.4. The extrapolation factors are computed as the ratios of the predicted cross-sections integrated over $0 < p_T < 8$ GeV/c and $2.0 < y < 4.5$ to the predicted cross-sections integrated over the well measured bins for each of four tunes of PYTHIA 6.4: LHCb-tune [17], Perugia 0, Perugia NOCR, and Perugia 2010 [30]. The mean of these four ratios is used as a multiplicative factor to extrapolate the sum of the well measured bins to the full kinematic range under study. The root mean

Table 2
Open charm production cross-sections in the kinematic range $0 < p_T < 8$ GeV/c and $2.0 < y < 4.5$. The computation of the extrapolation factors is described in the text. The first uncertainty is statistical, the second is systematic, and the third is the contribution from the extrapolation factor.

	Extrapolation factor	Cross-section (μb)
D^0	1.003 ± 0.001	$1661 \pm 16 \pm 128 \pm 2$
D^+	1.067 ± 0.013	$645 \pm 11 \pm 72 \pm 8$
D^{*+}	1.340 ± 0.037	$677 \pm 26 \pm 77 \pm 19$
D_s^+	1.330 ± 0.056	$197 \pm 14 \pm 26 \pm 8$
Λ_c^+	1.311 ± 0.077	$233 \pm 26 \pm 71 \pm 14$

Table 3
Correlation matrix of the uncertainties of the integrated open charm production cross-sections in the kinematic range $0 < p_T < 8$ GeV/c and $2.0 < y < 4.5$. The first column restates measured values of the integrated cross-sections.

	$\sigma(D^0)$	$\sigma(D^+)$	$\sigma(D^{*+})$	$\sigma(D_s^+)$
$\sigma(D^0) = 1661 \pm 129$ μb				
$\sigma(D^+) = 645 \pm 74$ μb	0.76			
$\sigma(D^{*+}) = 677 \pm 83$ μb	0.77	0.73		
$\sigma(D_s^+) = 197 \pm 31$ μb	0.55	0.52	0.53	
$\sigma(\Lambda_c^+) = 233 \pm 77$ μb	0.26	0.25	0.25	0.18

Table 4
Cross-section ratios for open charm production in the kinematic range $0 < p_T < 8$ GeV/c and $2.0 < y < 4.5$. The numbers in the table are the ratios of the respective row/column.

	$\sigma(D^0)$	$\sigma(D^+)$	$\sigma(D^{*+})$	$\sigma(D_s^+)$
$\sigma(D^+)$	0.389 ± 0.029			
$\sigma(D^{*+})$	0.407 ± 0.033	1.049 ± 0.092		
$\sigma(D_s^+)$	0.119 ± 0.016	0.305 ± 0.042	0.291 ± 0.041	
$\sigma(\Lambda_c^+)$	0.140 ± 0.045	0.361 ± 0.116	0.344 ± 0.111	1.183 ± 0.402

square of the four ratios is taken as a systematic uncertainty associated with the extrapolation. We confirm that this procedure gives uncertainties of appropriate size by examining the variance of the ratios for individual well measured bins. The resulting integrated cross-sections for each hadron species are given in Table 2.

Accounting for the correlations among the sources of systematic uncertainty, we obtain the correlation matrix for the total uncertainties of the integrated cross-section measurements shown in Table 3. The ratios of the production cross-sections in the kinematic range $0 < p_T < 8$ GeV/c and $2.0 < y < 4.5$ are given in Table 4.

Finally, we determine the total charm cross-section contributing to charmed hadron production inside the acceptance of this study, $0 < p_T < 8$ GeV/c and $2.0 < y < 4.5$. Combining our measurements $\sigma(H_c)$ with the corresponding fragmentation functions $f(c \to H_c)$ from Ref. [27] gives five estimates of $\sigma(c\bar{c}) = \sigma(H_c)/(2f(c \to H_c))$. The factor of 2 appears in the denominator because we have defined $\sigma(H_c)$ to be the cross-section to produce either H_c or its charge conjugate. A combination of all five measurements taking correlations into account gives

$$\sigma(c\bar{c})_{p_T<8\ \mathrm{GeV}/c,\ 2.0<y<4.5} = 1419 \pm 12\,(\mathrm{stat}) \pm 116\,(\mathrm{syst}) \pm 65\,(\mathrm{frag})\ \mu\mathrm{b}.$$

The final uncertainty is that due to the fragmentation functions.

6. Summary

A measurement of charm production in pp collisions at a centre-of-mass energy of 7 TeV has been performed with the LHCb detector, based on an integrated luminosity of $\mathcal{L}_{\mathrm{int}} = 15\ \mathrm{nb}^{-1}$. Cross-section measurements with total uncertainties below 20% have been achieved. The shape and absolute normalisation of the differential cross-sections for $D^0/\overline{D}^0$, $D^{\pm}$, $D^{*\pm}$, $D_s^{\pm}$, and $\Lambda_c^{\pm}$ hadrons are found to be in agreement with theoretical predictions. The ratios of the production cross-sections for the five species under study have been measured. The $c\bar{c}$ cross-section for producing a charmed hadron in the range $0 < p_T < 8\ \mathrm{GeV}/c$ and $2.0 < y < 4.5$ is found to be $1419 \pm 12\,(\mathrm{stat}) \pm 116\,(\mathrm{syst}) \pm 65\,(\mathrm{frag})\ \mu\mathrm{b}$.

Acknowledgements

The authors are grateful to H. Spiesberger, B.A. Kniehl, G. Kramer, and I. Schienbein for providing theoretical cross-section predictions from the Generalized Mass Variable Flavour Number Scheme (GMVFNS). We thank M. Mangano, M. Cacciari, S. Frixione, M. Nason, and G. Ridolfi for supplying theoretical cross-section predictions using the Fixed Order Next to Leading Logarithm (FONLL) approach.

We express our gratitude to our colleagues in the CERN accelerator departments for the excellent performance of the LHC. We thank the technical and administrative staff at the LHCb institutes. We acknowledge support from CERN and from the national agencies: CAPES, CNPq, FAPERJ and FINEP (Brazil); NSFC (China); CNRS/IN2P3 and Region Auvergne (France); BMBF, DFG, HGF and MPG (Germany); SFI (Ireland); INFN (Italy); FOM and NWO (The Netherlands); SCSR (Poland); ANCS/IFA (Romania); MinES, Rosatom, RFBR and NRC "Kurchatov Institute" (Russia); MinECo, XuntaGal and GENCAT (Spain); SNSF and SER (Switzerland); NAS Ukraine (Ukraine); STFC (United Kingdom); NSF (USA).

We also acknowledge the support received from the ERC under FP7. The Tier1 computing centres are supported by IN2P3 (France), KIT and BMBF (Germany), INFN (Italy), NWO and SURF (The Netherlands), PIC (Spain), GridPP (United Kingdom).

We are thankful for the computing resources put at our disposal by Yandex LLC (Russia), as well as to the communities behind the multiple open source software packages that we depend on.

Appendix A. Measured open charm cross-sections

Table 5 shows the production cross-sections for Λ_c^+ baryons integrated over $2 < p_T < 8\ \mathrm{GeV}/c$ and over the rapidity range of the y bins. The differential production cross-section values (integrated over the y range of the respective bin) plotted in Figs. 4–5 are given in Tables 6–10.

Table 5
Bin-integrated production cross-sections in μb for prompt $\Lambda_c^+ +$ c.c. baryons in bins of y integrated over the range $2 < p_T < 8$ GeV/c. The first uncertainty is statistical, and the second is the total systematic.

p_T (GeV/c)	y			
	(2.0, 2.5)	(2.5, 3.0)	(3.0, 3.5)	(3.5, 4.0)
(2, 8)	$21.4 \pm 8.1 \pm 7.2$	$49.9 \pm 11.6 \pm 15.6$	$62.9 \pm 7.0 \pm 18.8$	$44.2 \pm 8.6 \pm 13.2$

Table 6
Differential production cross-sections, $d\sigma/dp_T$, in μb/(GeV/c) for prompt $\Lambda_c^+ +$ c.c. baryons in bins of p_T integrated over the rapidity range $2.0 < y < 4.5$. The first uncertainty is statistical, and the second is the total systematic.

p_T (GeV/c)	y
	(2.0, 4.5)
(2, 3)	$89.6 \pm 17.8 \pm 32.6$
(3, 4)	$49.8 \pm 7.9 \pm 15.3$
(4, 5)	$22.5 \pm 3.1 \pm 6.9$
(5, 6)	$8.5 \pm 1.4 \pm 2.6$
(6, 7)	$4.9 \pm 0.9 \pm 1.5$
(7, 8)	$2.4 \pm 0.6 \pm 0.8$

Table 7
Differential production cross-sections, $d\sigma/dp_T$, in μb/(GeV/c) for prompt $D^0 +$ c.c. mesons in bins of (p_T, y). The first uncertainty is statistical, and the second is the total systematic.

p_T (GeV/c)	y				
	(2.0, 2.5)	(2.5, 3.0)	(3.0, 3.5)	(3.5, 4.0)	(4.0, 4.5)
(0, 1)	$113.58 \pm 5.45 \pm 10.45$	$96.51 \pm 3.49 \pm 8.10$	$90.99 \pm 3.67 \pm 7.24$	$80.41 \pm 4.19 \pm 6.30$	$57.37 \pm 5.37 \pm 5.10$
(1, 2)	$147.06 \pm 5.78 \pm 12.45$	$146.54 \pm 4.08 \pm 12.16$	$129.43 \pm 3.89 \pm 10.19$	$112.64 \pm 4.52 \pm 8.95$	$81.57 \pm 5.20 \pm 7.02$
(2, 3)	$85.95 \pm 3.18 \pm 6.80$	$82.07 \pm 2.10 \pm 6.58$	$68.48 \pm 1.90 \pm 5.40$	$58.25 \pm 2.02 \pm 4.70$	$39.87 \pm 2.56 \pm 3.78$
(3, 4)	$41.79 \pm 1.78 \pm 3.82$	$34.86 \pm 1.10 \pm 2.82$	$31.30 \pm 1.05 \pm 2.47$	$22.65 \pm 1.00 \pm 2.13$	$15.50 \pm 1.29 \pm 1.51$
(4, 5)	$18.61 \pm 0.98 \pm 1.73$	$16.11 \pm 0.67 \pm 1.49$	$14.36 \pm 0.66 \pm 1.15$	$9.89 \pm 0.62 \pm 0.94$	$5.69 \pm 0.87 \pm 0.60$
(5, 6)	$9.35 \pm 0.66 \pm 0.90$	$8.85 \pm 0.48 \pm 0.84$	$6.23 \pm 0.41 \pm 0.60$	$4.88 \pm 0.43 \pm 0.48$	$3.22 \pm 0.98 \pm 0.46$
(6, 7)	$4.92 \pm 0.51 \pm 0.49$	$4.31 \pm 0.38 \pm 0.43$	$2.99 \pm 0.33 \pm 0.30$	$2.33 \pm 0.34 \pm 0.25$	
(7, 8)	$2.34 \pm 0.42 \pm 0.26$	$2.41 \pm 0.36 \pm 0.26$	$1.25 \pm 0.27 \pm 0.14$	$1.14 \pm 0.35 \pm 0.16$	

Table 8
Differential production cross-sections, $d\sigma/dp_T$, in μb/(GeV/c) for prompt $D^+ +$ c.c. mesons in bins of (p_T, y). The first uncertainty is statistical, and the second is the total systematic.

p_T (GeV/c)	y				
	(2.0, 2.5)	(2.5, 3.0)	(3.0, 3.5)	(3.5, 4.0)	(4.0, 4.5)
(0, 1)		$42.11 \pm 2.92 \pm 7.21$	$34.00 \pm 1.78 \pm 6.29$	$29.32 \pm 1.89 \pm 5.52$	$24.01 \pm 2.94 \pm 5.45$
(1, 2)	$55.56 \pm 6.79 \pm 9.89$	$52.72 \pm 2.27 \pm 8.31$	$50.74 \pm 1.66 \pm 7.68$	$45.26 \pm 1.70 \pm 7.56$	$32.87 \pm 2.47 \pm 6.59$
(2, 3)	$29.86 \pm 2.38 \pm 4.40$	$31.79 \pm 1.09 \pm 4.57$	$29.03 \pm 0.87 \pm 3.99$	$23.09 \pm 0.84 \pm 3.45$	$15.79 \pm 1.17 \pm 3.43$
(3, 4)	$14.97 \pm 1.04 \pm 2.14$	$15.69 \pm 0.57 \pm 2.10$	$13.53 \pm 0.48 \pm 1.71$	$10.15 \pm 0.45 \pm 1.49$	$5.84 \pm 0.55 \pm 1.25$
(4, 5)	$7.26 \pm 0.54 \pm 1.01$	$7.44 \pm 0.33 \pm 0.96$	$5.89 \pm 0.27 \pm 0.74$	$4.12 \pm 0.26 \pm 0.65$	$2.31 \pm 0.32 \pm 0.50$
(5, 6)	$3.37 \pm 0.31 \pm 0.58$	$3.51 \pm 0.21 \pm 0.46$	$2.81 \pm 0.18 \pm 0.36$	$1.90 \pm 0.16 \pm 0.31$	$0.64 \pm 0.18 \pm 0.14$
(6, 7)	$1.93 \pm 0.21 \pm 0.31$	$1.73 \pm 0.14 \pm 0.23$	$1.81 \pm 0.14 \pm 0.36$	$0.80 \pm 0.10 \pm 0.17$	
(7, 8)	$1.22 \pm 0.17 \pm 0.22$	$0.94 \pm 0.11 \pm 0.13$	$0.70 \pm 0.09 \pm 0.14$	$0.32 \pm 0.07 \pm 0.07$	

Table 9
Differential production cross-sections, $\mathrm{d}\sigma/\mathrm{d}p_{\mathrm{T}}$, in μb/(GeV/$c$) for prompt D^{*+} + c.c. mesons in bins of (p_{T}, y). The first uncertainty is statistical, and the second is the total systematic.

p_{T} (GeV/c)	y				
	(2.0, 2.5)	(2.5, 3.0)	(3.0, 3.5)	(3.5, 4.0)	(4.0, 4.5)
(0, 1)			$26.17 \pm 5.17 \pm 3.25$	$36.67 \pm 6.02 \pm 4.53$	$46.60 \pm 12.77 \pm 6.88$
(1, 2)		$62.56 \pm 8.42 \pm 7.91$	$49.02 \pm 3.13 \pm 5.73$	$39.27 \pm 3.15 \pm 4.62$	$32.40 \pm 4.41 \pm 4.06$
(2, 3)		$30.60 \pm 2.85 \pm 3.66$	$24.93 \pm 1.54 \pm 2.91$	$24.11 \pm 1.77 \pm 2.86$	$18.55 \pm 2.37 \pm 2.45$
(3, 4)	$15.31 \pm 3.11 \pm 2.12$	$17.11 \pm 1.37 \pm 2.04$	$13.90 \pm 0.93 \pm 1.63$	$10.44 \pm 0.91 \pm 1.34$	$5.13 \pm 1.06 \pm 0.70$
(4, 5)	$9.90 \pm 1.61 \pm 1.35$	$6.28 \pm 0.66 \pm 0.81$	$6.20 \pm 0.57 \pm 0.74$	$4.51 \pm 0.53 \pm 0.59$	$3.41 \pm 1.02 \pm 0.52$
(5, 6)	$3.92 \pm 0.84 \pm 0.55$	$3.81 \pm 0.47 \pm 0.50$	$3.43 \pm 0.42 \pm 0.45$	$1.96 \pm 0.35 \pm 0.27$	
(6, 7)	$2.40 \pm 0.59 \pm 0.36$	$1.78 \pm 0.32 \pm 0.24$	$1.05 \pm 0.25 \pm 0.15$	$0.68 \pm 0.24 \pm 0.10$	
(7, 8)	$1.74 \pm 0.58 \pm 0.30$	$1.10 \pm 0.31 \pm 0.17$			

Table 10
Differential production cross-sections, $\mathrm{d}\sigma/\mathrm{d}p_{\mathrm{T}}$, in μb/(GeV/$c$) for prompt D_s^+ + c.c. mesons in bins of (p_{T}, y). The first uncertainty is statistical, and the second is the total systematic.

p_{T} (GeV/c)	y				
	(2.0, 2.5)	(2.5, 3.0)	(3.0, 3.5)	(3.5, 4.0)	(4.0, 4.5)
(0, 1)			$11.23 \pm 3.64 \pm 2.48$		
(1, 2)	$22.50 \pm 7.79 \pm 6.09$	$20.41 \pm 3.07 \pm 3.53$	$12.04 \pm 2.10 \pm 2.36$	$11.00 \pm 3.09 \pm 2.61$	
(2, 3)	$6.03 \pm 1.88 \pm 1.43$	$8.34 \pm 1.17 \pm 1.17$	$10.37 \pm 1.18 \pm 1.46$	$7.34 \pm 1.31 \pm 1.22$	$5.89 \pm 2.22 \pm 1.42$
(3, 4)	$3.38 \pm 0.92 \pm 0.66$	$5.57 \pm 0.73 \pm 0.81$	$4.78 \pm 0.69 \pm 0.79$	$3.83 \pm 0.68 \pm 0.65$	$2.08 \pm 0.90 \pm 0.49$
(4, 5)	$1.79 \pm 0.50 \pm 0.31$	$2.18 \pm 0.37 \pm 0.30$	$1.49 \pm 0.29 \pm 0.21$	$1.62 \pm 0.39 \pm 0.26$	
(5, 6)	$0.91 \pm 0.34 \pm 0.20$	$1.11 \pm 0.24 \pm 0.17$	$0.88 \pm 0.21 \pm 0.13$	$0.67 \pm 0.21 \pm 0.13$	
(6, 7)	$0.68 \pm 0.23 \pm 0.15$	$0.51 \pm 0.16 \pm 0.08$	$0.62 \pm 0.18 \pm 0.10$		
(7, 8)	$0.60 \pm 0.21 \pm 0.14$		$0.23 \pm 0.10 \pm 0.04$		

References

[1] B.A. Kniehl, G. Kramer, I. Schienbein, H. Spiesberger, Inclusive $D^{*\pm}$ production in $p\bar{p}$ collisions with massive charm quarks, Phys. Rev. D 71 (2005) 014018, arXiv:hep-ph/0410289.
[2] B.A. Kniehl, G. Kramer, D^0, D^+, D_s^+, and Λ_c^+ fragmentation functions from CERN LEP1, Phys. Rev. D 71 (2005) 094013, arXiv:hep-ph/0504058.
[3] B.A. Kniehl, G. Kramer, I. Schienbein, H. Spiesberger, Reconciling open charm production at the Fermilab Tevatron with QCD, Phys. Rev. Lett. 96 (2006) 012001, arXiv:hep-ph/0508129.
[4] T. Kneesch, B.A. Kniehl, G. Kramer, I. Schienbein, Charmed-meson fragmentation functions with finite-mass corrections, Nucl. Phys. B 799 (2008) 34, arXiv:0712.0481.
[5] B.A. Kniehl, G. Kramer, I. Schienbein, H. Spiesberger, Open charm hadroproduction and the charm content of the proton, Phys. Rev. D 79 (2009) 094009, arXiv:0901.4130.
[6] B. Kniehl, G. Kramer, I. Schienbein, H. Spiesberger, Inclusive charmed-meson production at the CERN LHC, Eur. Phys. J. C 72 (2012) 2082, arXiv:1202.0439.
[7] M. Cacciari, M. Greco, P. Nason, The p_{T} spectrum in heavy-flavour hadroproduction, JHEP 9805 (1998) 007, arXiv:hep-ph/9803400.
[8] M. Cacciari, P. Nason, Charm cross-sections for the Tevatron Run II, JHEP 0309 (2003) 006, arXiv:hep-ph/0306212.
[9] M. Cacciari, P. Nason, C. Oleari, A study of heavy flavoured meson fragmentation functions in e^+e^- annihilation, JHEP 0604 (2006) 006, arXiv:hep-ph/0510032.
[10] M. Cacciari, et al., Theoretical predictions for charm and bottom production at the LHC, JHEP 1210 (2012) 137, arXiv:1205.6344.
[11] CDF Collaboration, D. Acosta, et al., Measurement of prompt charm meson production cross sections in $p\bar{p}$ collisions at $\sqrt{s} = 1.96$ TeV, Phys. Rev. Lett. 91 (2003) 241804, arXiv:hep-ex/0307080.

[12] ALICE Collaboration, B. Abelev, et al., Measurement of charm production at central rapidity in proton–proton collisions at $\sqrt{s} = 2.76$ TeV, JHEP 1207 (2012) 191, arXiv:1205.4007.
[13] ALICE Collaboration, B. Abelev, et al., D_s^+ meson production at central rapidity in proton–proton collisions at $\sqrt{s} = 7$ TeV, Phys. Lett. B 718 (2012) 279, arXiv:1208.1948.
[14] ALICE Collaboration, B. Abelev, et al., Measurement of charm production at central rapidity in proton–proton collisions at $\sqrt{s} = 7$ TeV, JHEP 1201 (2012) 128, arXiv:1111.1553.
[15] LHCb Collaboration, A.A. Alves Jr., et al., The LHCb detector at the LHC, JINST 3 (2008) S08005.
[16] T. Sjöstrand, S. Mrenna, P. Skands, PYTHIA 6.4 physics and manual, JHEP 0605 (2006) 026, arXiv:hep-ph/0603175.
[17] I. Belyaev, et al., Handling of the generation of primary events in GAUSS, the LHCb simulation framework, Nuclear Science Symposium Conference Record (NSS/MIC), IEEE (2010) 1155.
[18] J. Pumplin, et al., New generation of parton distributions with uncertainties from global QCD analysis, JHEP 0207 (2002) 012, arXiv:hep-ph/0201195.
[19] D.J. Lange, The EvtGen particle decay simulation package, Nucl. Instrum. Meth. A 462 (2001) 152.
[20] P. Golonka, Z. Was, PHOTOS Monte Carlo: a precision tool for QED corrections in Z and W decays, Eur. Phys. J. C 45 (2006) 97, arXiv:hep-ph/0506026.
[21] GEANT4 Collaboration, J. Allison, et al., Geant4 developments and applications, IEEE Trans. Nucl. Sci. 53 (2006) 270;
GEANT4 Collaboration, S. Agostinelli, et al., GEANT4: a simulation toolkit, Nucl. Instrum. Meth. A 506 (2003) 250.
[22] M. Clemencic, et al., The LHCb simulation application, GAUSS: design, evolution and experience, J. Phys.: Conf. Ser. 331 (2011) 032023.
[23] Particle Data Group, J. Beringer, et al., Review of particle physics, Phys. Rev. D 86 (2012) 010001.
[24] T. Skwarnicki, A study of the radiative cascade transitions between the Upsilon-prime and Upsilon resonances, PhD thesis, Institute of Nuclear Physics, Krakow, 1986, DESY-F31-86-02.
[25] CLEO Collaboration, J.P. Alexander, et al., Absolute measurement of hadronic branching fractions of the D_s^+ meson, Phys. Rev. Lett. 100 (2008) 161804, arXiv:0801.0680.
[26] P.M. Nadolsky, et al., Implications of CTEQ global analysis for collider observables, Phys. Rev. D 78 (2008) 013004, arXiv:0802.0007.
[27] Particle Data Group, C. Amsler, et al., Review of particle physics, Phys. Lett. B 667 (2008) 1.
[28] W. Tung, et al., Heavy quark mass effects in deep inelastic scattering and global QCD analysis, JHEP 0702 (2007) 053, arXiv:hep-ph/0611254.
[29] J. Pumplin, H.L. Lai, W.K. Tung, The charm parton content of the nucleon, Phys. Rev. D 75 (2007) 054029, arXiv:hep-ph/0701220.
[30] P.Z. Skands, Tuning Monte Carlo generators: the Perugia tunes, Phys. Rev. D 82 (2010) 074018, and updates in arXiv:1005.3457.

LHCb Collaboration

R. Aaij [38], C. Abellan Beteta [33,n], A. Adametz [11], B. Adeva [34], M. Adinolfi [43], C. Adrover [6], A. Affolder [49], Z. Ajaltouni [5], J. Albrecht [9], F. Alessio [35], M. Alexander [48], S. Ali [38], G. Alkhazov [27], P. Alvarez Cartelle [34], A.A. Alves Jr. [22,35], S. Amato [2], Y. Amhis [7], L. Anderlini [17,f], J. Anderson [37], R. Andreassen [56], R.B. Appleby [51], O. Aquines Gutierrez [10], F. Archilli [18], A. Artamonov [32], M. Artuso [53], E. Aslanides [6], G. Auriemma [22,m], S. Bachmann [11], J.J. Back [45], C. Baesso [54], V. Balagura [28], W. Baldini [16], R.J. Barlow [51], C. Barschel [35], S. Barsuk [7], W. Barter [44], Th. Bauer [38], A. Bay [36], J. Beddow [48], I. Bediaga [1], S. Belogurov [28], K. Belous [32], I. Belyaev [28], E. Ben-Haim [8], M. Benayoun [8], G. Bencivenni [18], S. Benson [47], J. Benton [43], A. Berezhnoy [29], R. Bernet [37], M.-O. Bettler [44], M. van Beuzekom [38],

A. Bien [11], S. Bifani [12], T. Bird [51], A. Bizzeti [17,h], P.M. Bjørnstad [51], T. Blake [35], F. Blanc [36], C. Blanks [50], J. Blouw [11], S. Blusk [53], A. Bobrov [31], V. Bocci [22], A. Bondar [31], N. Bondar [27], W. Bonivento [15], S. Borghi [51], A. Borgia [53], T.J.V. Bowcock [49], E. Bowen [37], C. Bozzi [16], T. Brambach [9], J. van den Brand [39], J. Bressieux [36], D. Brett [51], M. Britsch [10], T. Britton [53], N.H. Brook [43], H. Brown [49], I. Burducea [26], A. Bursche [37], J. Buytaert [35], S. Cadeddu [15], O. Callot [7], M. Calvi [20,j], M. Calvo Gomez [33,n], A. Camboni [33], P. Campana [18,35], A. Carbone [14,c], G. Carboni [21,k], R. Cardinale [19,i], A. Cardini [15], H. Carranza-Mejia [47], L. Carson [50], K. Carvalho Akiba [2], G. Casse [49], M. Cattaneo [35], Ch. Cauet [9], M. Charles [52], Ph. Charpentier [35], P. Chen [3,36], N. Chiapolini [37], M. Chrzaszcz [23], K. Ciba [35], X. Cid Vidal [34], G. Ciezarek [50], P.E.L. Clarke [47], M. Clemencic [35], H.V. Cliff [44], J. Closier [35], C. Coca [26], V. Coco [38], J. Cogan [6], E. Cogneras [5], P. Collins [35], A. Comerma-Montells [33], A. Contu [15], A. Cook [43], M. Coombes [43], G. Corti [35], B. Couturier [35], G.A. Cowan [36], D. Craik [45], S. Cunliffe [50], R. Currie [47], C. D'Ambrosio [35], P. David [8], P.N.Y. David [38], I. De Bonis [4], K. De Bruyn [38], S. De Capua [51], M. De Cian [37], J.M. De Miranda [1], L. De Paula [2], W. De Silva [56], P. De Simone [18], D. Decamp [4], M. Deckenhoff [9], H. Degaudenzi [36,35], L. Del Buono [8], C. Deplano [15], D. Derkach [14], O. Deschamps [5], F. Dettori [39], A. Di Canto [11], J. Dickens [44], H. Dijkstra [35], P. Diniz Batista [1], M. Dogaru [26], F. Domingo Bonal [33,n], S. Donleavy [49], F. Dordei [11], A. Dosil Suárez [34], D. Dossett [45], A. Dovbnya [40], F. Dupertuis [36], R. Dzhelyadin [32], A. Dziurda [23], A. Dzyuba [27], S. Easo [46,35], U. Egede [50], V. Egorychev [28], S. Eidelman [31], D. van Eijk [38], S. Eisenhardt [47], U. Eitschberger [9], R. Ekelhof [9], L. Eklund [48], I. El Rifai [5], Ch. Elsasser [37], D. Elsby [42], A. Falabella [14,e], C. Färber [11], G. Fardell [47], C. Farinelli [38], S. Farry [12], V. Fave [36], D. Ferguson [47], V. Fernandez Albor [34], F. Ferreira Rodrigues [1], M. Ferro-Luzzi [35], S. Filippov [30], C. Fitzpatrick [35], M. Fontana [10], F. Fontanelli [19,i], R. Forty [35], O. Francisco [2], M. Frank [35], C. Frei [35], M. Frosini [17,f], S. Furcas [20], E. Furfaro [21], A. Gallas Torreira [34], D. Galli [14,c], M. Gandelman [2], P. Gandini [52], Y. Gao [3], J. Garofoli [53], P. Garosi [51], J. Garra Tico [44], L. Garrido [33], C. Gaspar [35], R. Gauld [52], E. Gersabeck [11], M. Gersabeck [51], T. Gershon [45,35], Ph. Ghez [4], V. Gibson [44], V.V. Gligorov [35], C. Göbel [54], D. Golubkov [28], A. Golutvin [50,28,35], A. Gomes [2], H. Gordon [52], M. Grabalosa Gándara [5],

R. Graciani Diaz [33], L.A. Granado Cardoso [35], E. Graugés [33], G. Graziani [17], A. Grecu [26], E. Greening [52], S. Gregson [44], O. Grünberg [55], B. Gui [53], E. Gushchin [30], Yu. Guz [32], T. Gys [35], C. Hadjivasiliou [53], G. Haefeli [36], C. Haen [35], S.C. Haines [44], S. Hall [50], T. Hampson [43], S. Hansmann-Menzemer [11], N. Harnew [52], S.T. Harnew [43], J. Harrison [51], P.F. Harrison [45], T. Hartmann [55], J. He [7], V. Heijne [38], K. Hennessy [49], P. Henrard [5], J.A. Hernando Morata [34], E. van Herwijnen [35], E. Hicks [49], D. Hill [52], M. Hoballah [5], C. Hombach [51], P. Hopchev [4], W. Hulsbergen [38], P. Hunt [52], T. Huse [49], N. Hussain [52], D. Hutchcroft [49], D. Hynds [48], V. Iakovenko [41], P. Ilten [12], R. Jacobsson [35], A. Jaeger [11], E. Jans [38], F. Jansen [38], P. Jaton [36], F. Jing [3], M. John [52], D. Johnson [52], C.R. Jones [44], B. Jost [35], M. Kaballo [9], S. Kandybei [40], M. Karacson [35], T.M. Karbach [35], I.R. Kenyon [42], U. Kerzel [35], T. Ketel [39], A. Keune [36], B. Khanji [20], O. Kochebina [7], I. Komarov [36,29], R.F. Koopman [39], P. Koppenburg [38], M. Korolev [29], A. Kozlinskiy [38], L. Kravchuk [30], K. Kreplin [11], M. Kreps [45], G. Krocker [11], P. Krokovny [31], F. Kruse [9], M. Kucharczyk [20,23,j], V. Kudryavtsev [31], T. Kvaratskheliya [28,35], V.N. La Thi [36], D. Lacarrere [35], G. Lafferty [51], A. Lai [15], D. Lambert [47], R.W. Lambert [39], E. Lanciotti [35], G. Lanfranchi [18,35], C. Langenbruch [35], T. Latham [45], C. Lazzeroni [42], R. Le Gac [6], J. van Leerdam [38], J.-P. Lees [4], R. Lefèvre [5], A. Leflat [29,35], J. Lefrançois [7], O. Leroy [6], Y. Li [3], L. Li Gioi [5], M. Liles [49], R. Lindner [35], C. Linn [11], B. Liu [3], G. Liu [35], J. von Loeben [20], J.H. Lopes [2], E. Lopez Asamar [33], N. Lopez-March [36], H. Lu [3], J. Luisier [36], H. Luo [47], F. Machefert [7], I.V. Machikhiliyan [4,28], F. Maciuc [26], O. Maev [27,35], S. Malde [52], G. Manca [15,d], G. Mancinelli [6], N. Mangiafave [44], U. Marconi [14], R. Märki [36], J. Marks [11], G. Martellotti [22], A. Martens [8], L. Martin [52], A. Martín Sánchez [7], M. Martinelli [38], D. Martinez Santos [39], D. Martins Tostes [2], A. Massafferri [1], R. Matev [35], Z. Mathe [35], C. Matteuzzi [20], M. Matveev [27], E. Maurice [6], A. Mazurov [16,30,35,e], J. McCarthy [42], R. McNulty [12], B. Meadows [56,52], F. Meier [9], M. Meissner [11], M. Merk [38], D.A. Milanes [13], M.-N. Minard [4], J. Molina Rodriguez [54], S. Monteil [5], D. Moran [51], P. Morawski [23], R. Mountain [53], I. Mous [38], F. Muheim [47], K. Müller [37], R. Muresan [26], B. Muryn [24], B. Muster [36], P. Naik [43], T. Nakada [36], R. Nandakumar [46], I. Nasteva [1], M. Needham [47], N. Neufeld [35], A.D. Nguyen [36], T.D. Nguyen [36], C. Nguyen-Mau [36,o], M. Nicol [7], V. Niess [5], R. Niet [9], N. Nikitin [29], T. Nikodem [11], A. Nomerotski [52], A. Novoselov [32],

A. Oblakowska-Mucha [24], V. Obraztsov [32], S. Oggero [38], S. Ogilvy [48], O. Okhrimenko [41], R. Oldeman [15,35,d], M. Orlandea [26], J.M. Otalora Goicochea [2], P. Owen [50], B.K. Pal [53], A. Palano [13,b], M. Palutan [18], J. Panman [35], A. Papanestis [46], M. Pappagallo [48], C. Parkes [51], C.J. Parkinson [50], G. Passaleva [17], G.D. Patel [49], M. Patel [50], G.N. Patrick [46], C. Patrignani [19,i], C. Pavel-Nicorescu [26], A. Pazos Alvarez [34], A. Pellegrino [38], G. Penso [22,l], M. Pepe Altarelli [35], S. Perazzini [14,c], D.L. Perego [20,j], E. Perez Trigo [34], A. Pérez-Calero Yzquierdo [33], P. Perret [5], M. Perrin-Terrin [6], G. Pessina [20], K. Petridis [50], A. Petrolini [19,i], A. Phan [53], E. Picatoste Olloqui [33], B. Pietrzyk [4], T. Pilař [45], D. Pinci [22], S. Playfer [47], M. Plo Casasus [34], F. Polci [8], G. Polok [23], A. Poluektov [45,31], E. Polycarpo [2], D. Popov [10], B. Popovici [26], C. Potterat [33], A. Powell [52], J. Prisciandaro [36], V. Pugatch [41], A. Puig Navarro [36], W. Qian [4], J.H. Rademacker [43], B. Rakotomiaramanana [36], M.S. Rangel [2], I. Raniuk [40], N. Rauschmayr [35], G. Raven [39], S. Redford [52], M.M. Reid [45], A.C. dos Reis [1], S. Ricciardi [46], A. Richards [50], K. Rinnert [49], V. Rives Molina [33], D.A. Roa Romero [5], P. Robbe [7], E. Rodrigues [51], P. Rodriguez Perez [34], G.J. Rogers [44], S. Roiser [35], V. Romanovsky [32], A. Romero Vidal [34], J. Rouvinet [36], T. Ruf [35], H. Ruiz [33], G. Sabatino [22,k], J.J. Saborido Silva [34], N. Sagidova [27], P. Sail [48], B. Saitta [15,d], C. Salzmann [37], B. Sanmartin Sedes [34], M. Sannino [19,i], R. Santacesaria [22], C. Santamarina Rios [34], E. Santovetti [21,k], M. Sapunov [6], A. Sarti [18,l], C. Satriano [22,m], A. Satta [21], M. Savrie [16,e], D. Savrina [28,29], P. Schaack [50], M. Schiller [39], H. Schindler [35], S. Schleich [9], M. Schlupp [9], M. Schmelling [10], B. Schmidt [35], O. Schneider [36], A. Schopper [35], M.-H. Schune [7], R. Schwemmer [35], B. Sciascia [18], A. Sciubba [18,l], M. Seco [34], A. Semennikov [28], K. Senderowska [24], I. Sepp [50], N. Serra [37], J. Serrano [6], P. Seyfert [11], M. Shapkin [32], I. Shapoval [40,35], P. Shatalov [28], Y. Shcheglov [27], T. Shears [49,35], L. Shekhtman [31], O. Shevchenko [40], V. Shevchenko [28], A. Shires [50], R. Silva Coutinho [45], T. Skwarnicki [53], N.A. Smith [49], E. Smith [52,46], M. Smith [51], K. Sobczak [5], M.D. Sokoloff [56], F.J.P. Soler [48], F. Soomro [18,35], D. Souza [43], B. Souza De Paula [2], B. Spaan [9], A. Sparkes [47], P. Spradlin [48,*], F. Stagni [35], S. Stahl [11], O. Steinkamp [37], S. Stoica [26], S. Stone [53], B. Storaci [37], M. Straticiuc [26], U. Straumann [37], V.K. Subbiah [35], S. Swientek [9], V. Syropoulos [39], M. Szczekowski [25], P. Szczypka [36,35], T. Szumlak [24], S. T'Jampens [4],

M. Teklishyn [7], E. Teodorescu [26], F. Teubert [35], C. Thomas [52], E. Thomas [35], J. van Tilburg [11], V. Tisserand [4], M. Tobin [37], S. Tolk [39], D. Tonelli [35], S. Topp-Joergensen [52], N. Torr [52], E. Tournefier [4,50], S. Tourneur [36], M.T. Tran [36], M. Tresch [37], A. Tsaregorodtsev [6], P. Tsopelas [38], N. Tuning [38], M. Ubeda Garcia [35], A. Ukleja [25], D. Urner [51], U. Uwer [11], V. Vagnoni [14], G. Valenti [14], R. Vazquez Gomez [33], P. Vazquez Regueiro [34], S. Vecchi [16], J.J. Velthuis [43], M. Veltri [17,g], G. Veneziano [36], M. Vesterinen [35], B. Viaud [7], D. Vieira [2], X. Vilasis-Cardona [33,n], A. Vollhardt [37], D. Volyanskyy [10], D. Voong [43], A. Vorobyev [27], V. Vorobyev [31], C. Voß [55], H. Voss [10], R. Waldi [55], R. Wallace [12], S. Wandernoth [11], J. Wang [53], D.R. Ward [44], N.K. Watson [42], A.D. Webber [51], D. Websdale [50], M. Whitehead [45], J. Wicht [35], J. Wiechczynski [23], D. Wiedner [11], L. Wiggers [38], G. Wilkinson [52], M.P. Williams [45,46], M. Williams [50,p], F.F. Wilson [46], J. Wishahi [9], M. Witek [23], S.A. Wotton [44], S. Wright [44], S. Wu [3], K. Wyllie [35], Y. Xie [47,35], F. Xing [52], Z. Xing [53], Z. Yang [3], R. Young [47], X. Yuan [3], O. Yushchenko [32], M. Zangoli [14], M. Zavertyaev [10,a], F. Zhang [3], L. Zhang [53], W.C. Zhang [12], Y. Zhang [3], A. Zhelezov [11], A. Zhokhov [28], L. Zhong [3], A. Zvyagin [35]

[1] *Centro Brasileiro de Pesquisas Físicas (CBPF), Rio de Janeiro, Brazil*
[2] *Universidade Federal do Rio de Janeiro (UFRJ), Rio de Janeiro, Brazil*
[3] *Center for High Energy Physics, Tsinghua University, Beijing, China*
[4] *LAPP, Université de Savoie, CNRS/IN2P3, Annecy-Le-Vieux, France*
[5] *Clermont Université, Université Blaise Pascal, CNRS/IN2P3, LPC, Clermont-Ferrand, France*
[6] *CPPM, Aix-Marseille Université, CNRS/IN2P3, Marseille, France*
[7] *LAL, Université Paris-Sud, CNRS/IN2P3, Orsay, France*
[8] *LPNHE, Université Pierre et Marie Curie, Université Paris Diderot, CNRS/IN2P3, Paris, France*
[9] *Fakultät Physik, Technische Universität Dortmund, Dortmund, Germany*
[10] *Max-Planck-Institut für Kernphysik (MPIK), Heidelberg, Germany*
[11] *Physikalisches Institut, Ruprecht-Karls-Universität Heidelberg, Heidelberg, Germany*
[12] *School of Physics, University College Dublin, Dublin, Ireland*
[13] *Sezione INFN di Bari, Bari, Italy*
[14] *Sezione INFN di Bologna, Bologna, Italy*
[15] *Sezione INFN di Cagliari, Cagliari, Italy*
[16] *Sezione INFN di Ferrara, Ferrara, Italy*
[17] *Sezione INFN di Firenze, Firenze, Italy*
[18] *Laboratori Nazionali dell'INFN di Frascati, Frascati, Italy*
[19] *Sezione INFN di Genova, Genova, Italy*
[20] *Sezione INFN di Milano Bicocca, Milano, Italy*
[21] *Sezione INFN di Roma Tor Vergata, Roma, Italy*
[22] *Sezione INFN di Roma La Sapienza, Roma, Italy*
[23] *Henryk Niewodniczanski Institute of Nuclear Physics Polish Academy of Sciences, Kraków, Poland*
[24] *AGH University of Science and Technology, Kraków, Poland*
[25] *National Center for Nuclear Research (NCBJ), Warsaw, Poland*
[26] *Horia Hulubei National Institute of Physics and Nuclear Engineering, Bucharest-Magurele, Romania*
[27] *Petersburg Nuclear Physics Institute (PNPI), Gatchina, Russia*
[28] *Institute of Theoretical and Experimental Physics (ITEP), Moscow, Russia*

[29] *Institute of Nuclear Physics, Moscow State University (SINP MSU), Moscow, Russia*
[30] *Institute for Nuclear Research of the Russian Academy of Sciences (INR RAN), Moscow, Russia*
[31] *Budker Institute of Nuclear Physics (SB RAS) and Novosibirsk State University, Novosibirsk, Russia*
[32] *Institute for High Energy Physics (IHEP), Protvino, Russia*
[33] *Universitat de Barcelona, Barcelona, Spain*
[34] *Universidad de Santiago de Compostela, Santiago de Compostela, Spain*
[35] *European Organization for Nuclear Research (CERN), Geneva, Switzerland*
[36] *Ecole Polytechnique Fédérale de Lausanne (EPFL), Lausanne, Switzerland*
[37] *Physik-Institut, Universität Zürich, Zürich, Switzerland*
[38] *Nikhef National Institute for Subatomic Physics, Amsterdam, The Netherlands*
[39] *Nikhef National Institute for Subatomic Physics and VU University Amsterdam, Amsterdam, The Netherlands*
[40] *NSC Kharkiv Institute of Physics and Technology (NSC KIPT), Kharkiv, Ukraine*
[41] *Institute for Nuclear Research of the National Academy of Sciences (KINR), Kyiv, Ukraine*
[42] *University of Birmingham, Birmingham, United Kingdom*
[43] *H.H. Wills Physics Laboratory, University of Bristol, Bristol, United Kingdom*
[44] *Cavendish Laboratory, University of Cambridge, Cambridge, United Kingdom*
[45] *Department of Physics, University of Warwick, Coventry, United Kingdom*
[46] *STFC Rutherford Appleton Laboratory, Didcot, United Kingdom*
[47] *School of Physics and Astronomy, University of Edinburgh, Edinburgh, United Kingdom*
[48] *School of Physics and Astronomy, University of Glasgow, Glasgow, United Kingdom*
[49] *Oliver Lodge Laboratory, University of Liverpool, Liverpool, United Kingdom*
[50] *Imperial College London, London, United Kingdom*
[51] *School of Physics and Astronomy, University of Manchester, Manchester, United Kingdom*
[52] *Department of Physics, University of Oxford, Oxford, United Kingdom*
[53] *Syracuse University, Syracuse, NY, United States*
[54] *Pontifícia Universidade Católica do Rio de Janeiro (PUC-Rio), Rio de Janeiro, Brazil* [q]
[55] *Institut für Physik, Universität Rostock, Rostock, Germany* [r]
[56] *University of Cincinnati, Cincinnati, OH, United States* [s]

[*] Corresponding author.
E-mail address: patrick.spradlin@cern.ch (P. Spradlin).
[a] P.N. Lebedev Physical Institute, Russian Academy of Science (LPI RAS), Moscow, Russia.
[b] Università di Bari, Bari, Italy.
[c] Università di Bologna, Bologna, Italy.
[d] Università di Cagliari, Cagliari, Italy.
[e] Università di Ferrara, Ferrara, Italy.
[f] Università di Firenze, Firenze, Italy.
[g] Università di Urbino, Urbino, Italy.
[h] Università di Modena e Reggio Emilia, Modena, Italy.
[i] Università di Genova, Genova, Italy.
[j] Università di Milano Bicocca, Milano, Italy.
[k] Università di Roma Tor Vergata, Roma, Italy.
[l] Università di Roma La Sapienza, Roma, Italy.
[m] Università della Basilicata, Potenza, Italy.
[n] LIFAELS, La Salle, Universitat Ramon Llull, Barcelona, Spain.
[o] Hanoi University of Science, Hanoi, Viet Nam.
[p] Massachusetts Institute of Technology, Cambridge, MA, United States.
[q] Associated to Universidade Federal do Rio de Janeiro (UFRJ), Rio de Janeiro, Brazil.
[r] Associated to Physikalisches Institut, Ruprecht-Karls-Universität Heidelberg, Heidelberg, Germany.
[s] Associated to Syracuse University, Syracuse, NY, United States.